

PCCP

Accepted Manuscript



This is an *Accepted Manuscript*, which has been through the Royal Society of Chemistry peer review process and has been accepted for publication.

Accepted Manuscripts are published online shortly after acceptance, before technical editing, formatting and proof reading. Using this free service, authors can make their results available to the community, in citable form, before we publish the edited article. We will replace this *Accepted Manuscript* with the edited and formatted *Advance Article* as soon as it is available.

You can find more information about *Accepted Manuscripts* in the [Information for Authors](#).

Please note that technical editing may introduce minor changes to the text and/or graphics, which may alter content. The journal's standard [Terms & Conditions](#) and the [Ethical guidelines](#) still apply. In no event shall the Royal Society of Chemistry be held responsible for any errors or omissions in this *Accepted Manuscript* or any consequences arising from the use of any information it contains.



Cite this: DOI: 10.1039/xxxxxxxxxx

Photoinduced Charge-Transfer Dynamics Simulations in Noncovalently Bonded Molecular Aggregates[†]

Carlos R. Medrano,^a M. Belén Oviedo,^b and Cristián G. Sánchez^{*a}Received Date
Accepted Date

DOI: 10.1039/xxxxxxxxxx

www.rsc.org/journalname

The rational design of new materials as prototypes systems for organic solar cells remains challenging. Perylene diimide has emerged as a promising material to replace fullerene derivatives because of its synthetic flexibility, leading to the manipulation of their optical properties. As a result of their fused aromatic core that favors $\pi-\pi$ stacking interactions, the aggregation of these molecules can reach highly ordered nanostructures as one-dimensional nanofibers, with fast photoinduced charge transfer mechanism. In this article, we present an atomistic description of the photoexcited exciton dynamics in noncovalently bonded perylene diimides by time integration of the electron density in the presence of external time varying electric fields. We show that our approach is able to capture and explain the physics that underlies in the charge transport mechanism through perylene diimides aggregates.

1 Introduction

Over the past decades, organic semiconductor materials have received an increasing technological interest in the fabrication of field effect transistors (FETs)¹, organic photovoltaics (OPVs)² and organic light-emitting diodes (OLEDs)³. This interest is given by its numerous advantages such as easy and low cost of production, mechanical flexibility, tunable optical properties, among others⁴.

The most common design of an organic solar cell (OSC) consist of a blend (bulk heterojunction, BHJ) based on conjugated polymer electron donor (D) mixed with an electron acceptor material (A). This type of OSC are being intensively investigated in order to increase their efficiency achieving above 10% of power-conversion efficiencies (PCEs)^{5,6}. The basic operating principle of an OSC can be schematically described by the photon absorption and the creation of an exciton (electron-hole pair); followed by the exciton diffusion to the donor/acceptor interface and its dissociation creating a charge-transfer state; finally, the dissociation of the charge-transfer complex occurs leading to the generation of free charges carriers, where these free charges are transport within the organic semiconductor to the respective electrodes^{7,8}. For an efficient photogeneration of free charges carriers is require

an efficient dissociation of the exciton at the heterojunction or at the interface between a p-type and a n-type organic semiconductors.

Fullerenes and their derivatives, such as [6,6]-phenyl C₆₁ butyric acidmethyl ester (PC₆₁BM), have been the dominant electron acceptor materials in BHJ OSCs, due to their large electron affinity, high electron mobility and isotropy of charge transport^{9,10}. However, these material have some drawbacks like their inherently low LUMO energy levels compared with those of common donors resulting in energy loss², weak absorption in the visible spectral breadth, and band gap variability, which are difficult to tune in fullerene systems by chemical modification¹⁰. As an alternative to fullerene based acceptor materials, organic molecules based on non-fullerene acceptor materials have received attention in the past decades, because they can be easy be modified by tailoring the photofunctional backbone in order to tune the absorption spectrum and HOMO/LUMO energies¹¹.

3,4,9,10-perylenetetracarboxylic acid diimides (PDIs) and their derivatives (figure 1) are n-type organic semiconductors with high thermal, chemical and photochemical stabilities². In addition these molecules present high molar absorption coefficient in the visible region, strong electron-accepting ability and high electron mobility. By chemical modification in the molecule, their solubility and optical properties can be modulated. Given these outstanding chemical and physical properties, PDIs are a promising class of non-fullerene acceptor materials¹¹. On the other hand, their rigid, fused aromatic core favours $\pi-\pi$ intermolecular interactions imparting very ordered heterojunction structures and they are known to form one dimensional (1D) nanostructures¹². These nanofibers offer many potential advantages in de-

^aDepartamento de Matemática y Física, Facultad de Ciencias Químicas, INFIQC, Universidad Nacional de Córdoba, Ciudad Universitaria, X5000HUA, Córdoba, Argentina; E-mail: cgsanchez@fcq.unc.edu.ar

^bDepartment of Chemical & Environmental Engineering and Materials Science and Engineering Program, University of California, Riverside, California 92521, United States.

[†] Electronic Supplementary Information (ESI) available: [details of any supplementary information available should be included here]. See DOI: 10.1039/b000000x/

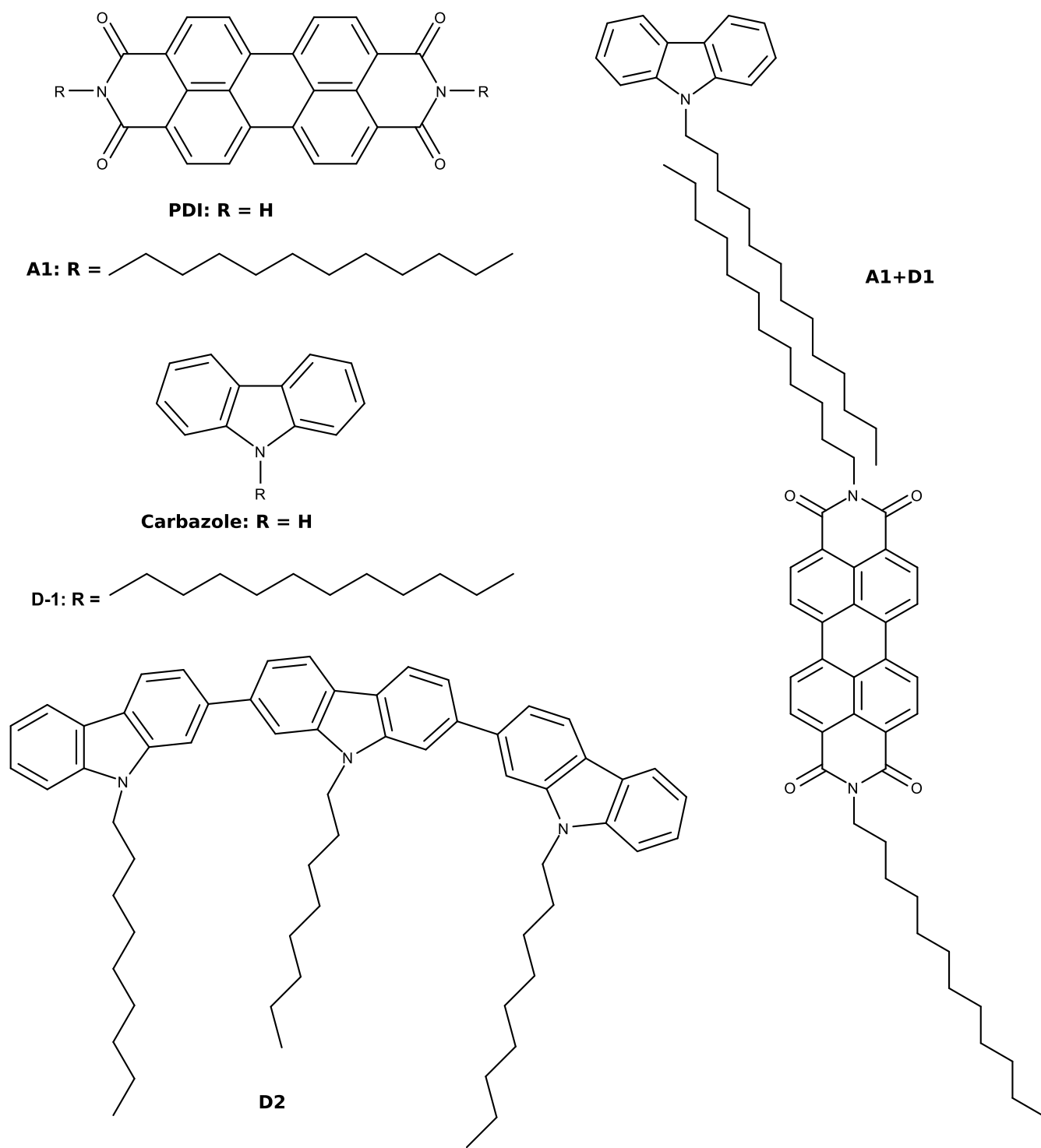


Fig. 1 (Left) Individual molecular structures of 3,4,9,10-perylenetetracarboxylic acid diimide (PDI) and carbazol derivatives. (Right) A1+D1 complex, where each component of the complex is interacting noncovalently through the hydrocarbon side chains.

veloping more efficient OSCs due to their larger exciton diffusion length, ultra-large D/A interface for exciton dissociation, and the controllable nanoscale morphology compared to BHJs based on fullerenes acceptors^{13,14}.

In a recent work by Zang and co-workers¹⁵ a simple method was informed for the assembly of organic nanofibril heterojunctions based on the interfacial engineering of carbazole derivatives coating onto PDI derivatives (figure 1). Both derivatives have long alkyl chains where these chains have a strong hydrophobic interaction. In particular, they reported a high photoconductivity and fast photoresponse with large on/off ratio. From the experimental data, the authors suggested that the high photocurrent is due to the presence of the alkyl groups where the recombination of photogenerated charge carriers are prevented.

In the present work we report a detailed analysis of the charge transfer process between different dyes and PDI aggregates through fully atomistic electron dynamics simulations. These simulations are based on real-time time-dependent density functional tight-binding (RT-TDDFTB) model which describes the system under non-equilibrium conditions. In particular, we shed light into the photoinduced charge transfer mechanism in these noncovalent bonded molecular nanostructures. We demonstrate that the alkyl side chains work as a *molecular wire* that tunes the interfacial electron transfer.

2 Computational Methods

The description of the electronic structure of carbazol, PDI and carbazol+PDI complex were described by a self-consistent density functional tight-binding Hamiltonian¹⁶. The method is based on the expansion of the Kohn-Sham energy functional up to second order with respect to a reference electron density for the neutral atoms. This method may be considered as an intermediate step between a full *ab-initio* calculation, where exchange and correlation energy are accounted in a simpler semi-empirical method. The DFTB+ code¹⁷ was used to obtain the optimization of the geometries as well as the calculations of the Hamiltonian, overlap matrix and the initial single electron density matrix. For the calculations performed here, we have used the *mio-1-1* parameter set for elements H, O, N, C and S^{16,18,19}.

This method is extended to the time-dependent SCC-DFTB (TD-DFTB)²⁰ to obtain the excited state properties of the system by applying a perturbation in the shape of a Dirac delta pulse to the initial ground-state density matrix previously obtained. After pulse application, the density matrix evolves in time and its evolution can be calculated by time integration of the Liouville-von Neumann equation of motion in the non-orthogonal basis, according to equation 1:

$$\frac{\partial \hat{\rho}}{\partial t} = -\frac{i}{\hbar} \left(S^{-1} \hat{H} [\hat{\rho}] \hat{\rho} - \hat{\rho} \hat{H} [\hat{\rho}] S^{-1} \right), \quad (1)$$

where $\hat{\rho}$ is the single electron density matrix, S^{-1} is the inverse of the overlap matrix and \hat{H} is the SCC-DFTB Hamiltonian. Within the linear response regime, when the applied electric field is small, the response is linear and the dipole moment is given by

equation 2:

$$\langle \mu(t) \rangle = \int_0^{\infty} \alpha(t-\tau) E(\tau) d\tau, \quad (2)$$

where $\alpha(t-\tau)$ is the polarizability along the axis over which the external field $\mathbf{E}(\tau)$ is applied. The absorption spectrum is proportional to the imaginary part of the frequency dependent polarizability (equation 3), obtained from the Fourier transform of the time-dependent dipole moment, after the deconvolution of the applied electric field.

$$\alpha(\omega) = \frac{\langle \mu(\omega) \rangle}{E(\omega)} \quad (3)$$

This method has been successfully used to calculate the optical properties of photosynthetic pigments^{20,21}, DNA intercalation complexes²² and organic molecules adsorbed onto TiO₂ nanoparticles²³. In these previous reports we showed that TD-DFTB based spectra showed a remarkable agreement with experimental results.

Recently, our group has studied the charge injection mechanism in dye-nanoparticles complexes²⁴⁻²⁶ in time domain, leading to good agreement with experimental results²⁶. The dynamics triggered by application of a continuous laser-type perturbation in tune with the excitation energy of interest. The charge transfer mechanism was monitored by computing the time-dependent Mulliken atomic charges. One of the advantage of our approach, based on the density matrix formalism along with the use of a self-consistent Hamiltonian, is that the method include the explicit description of electron-hole interactions.

For the visualization of molecular structures, movies and “coloring method” OVITO²⁷ and VMD^{28,29} packages were employed.

3 Results and Discussion

Table 1 Comparison of the absorption wavelength (nm) for carbazole and PDI in vacuum obtained by RT-TDDFTB simulations with the experimental values found in literature. The table shows the two longest-wavelength peaks for each molecule.

Carbazole		PDI	
Exp. value	RT-TDDFTB	Exp. value	RT-TDDFTB
335 ³⁰	323	526 ³¹	532
323 ³⁰	300	491 ³¹	510

The simulated absorption spectra of carbazol and PDI are displayed in figure 2 and the values of the lowest absorption energies for each molecule are shown in table 1. The absorption spectrum of each molecule were obtained after the deconvolution of the time-dependent dipole moment with the external field. The time-dependent dipole moment were calculated by a real-time propagation of the one-electron density matrix after the application of an initial perturbation in the shape of a delta Dirac, the intensity of this perturbation was 0.001 V/Å so the simulations are within the linear response regime. The time propagation of the density matrix is calculated by the numerical integration of equation 1 with a time step of 0.0048 fs and the simulation times were extended by at least 100 fs. From table 1 a good agreement can be

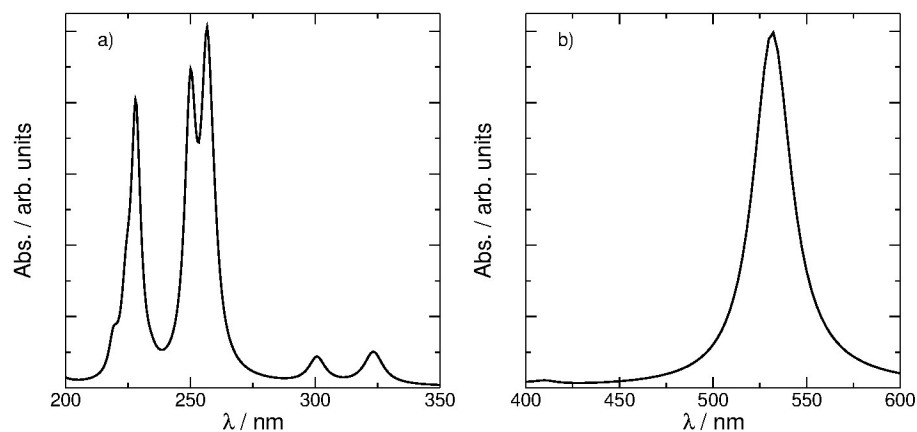


Fig. 2 Simulated absorption spectra for carbazole a) and PDI b).

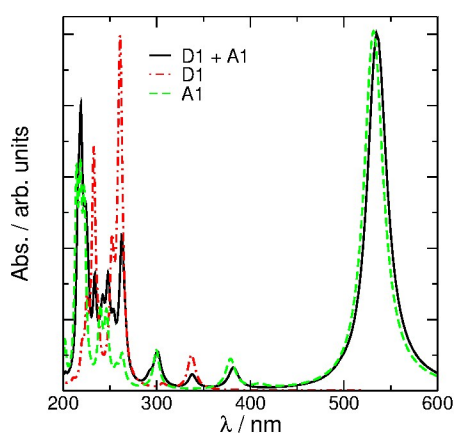


Fig. 3 Calculated absorption spectrum of D1+A1 (black, solid line), D1 (red, dash-dot line) and A1 (green, dashed line).

observed for the absorption energies of the calculation and experimental values. This first analysis of the absorption spectra is important to check the reliability of the quantum dynamics performed by this method.

Next, we build the donor+acceptor complex composed by D1 and A1 (see figure 1) and we optimize the full geometry using London dispersion forces³² in order to accurately describe the weak intermolecular interactions between the alkyl chains. Then, we calculate the absorption spectrum of the entire system as described above. Figure 3 shows the optical spectrum of D1+A1 complex and the spectra of the separate molecules. From this figure we can observe that the absorption spectrum of the complex is the sum of the donor and acceptor spectra, despite of the quantum nature of this calculation, where the state of the complex is the tensor product between the states of the donor and the acceptor, instead of the sum of the individual molecular states. This is the result of the weak coupling between the alkyl chains, hence a small deviation of the absorption energies can be observed and the main optical properties of each compound are not affected in the aggregate state.

Zang and co-workers¹⁵ proposed that the electron transfer in these aggregates via visible photostimulation, is caused by

Table 2 Highest Occupied Molecular Orbital (HOMO) and Lowest Unoccupied Molecular Orbital (LUMO) energies in eV for D1 and A1.

	HOMO	LUMO
D1	-5.32	-1.87
A1	-5.91	-4.19

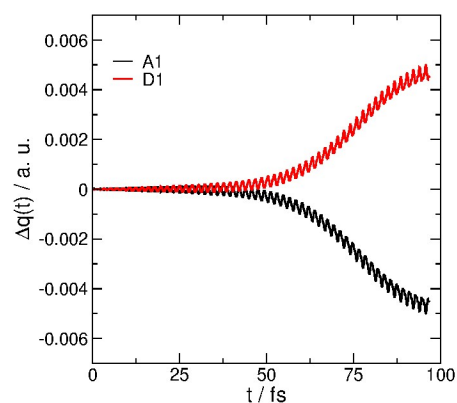


Fig. 4 Charge evolution of for D1+A1 in response to a laser illumination at 533 nm and with an intensity of 0.01V/Å.

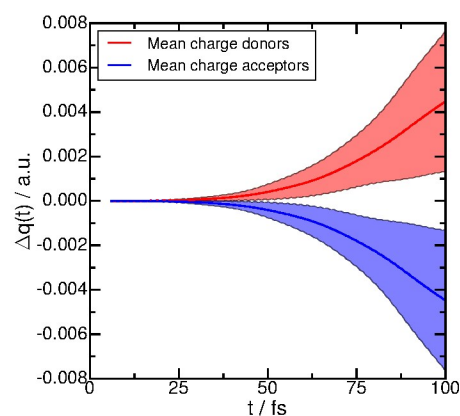


Fig. 5 Charge evolution for an ensemble of D1+A1 configurations in response to a laser illumination with an intensity of 0.01V/Å. The inner lines correspond to the mean charge of the acceptor and donor. The translucent surface represents the standard deviation of the ensemble mean (as $\bar{x} \pm \sigma$).

the proximity between the highest occupied molecular orbital (HOMO) of the donor and acceptor molecules, where the HOMO of D1 is slightly above the HOMO of A1. When the acceptor is excited, a hole in the HOMO is generated hence an electron from the HOMO of D1 can be injected to the acceptor. To corroborate this approach, we have calculated the HOMO and LUMO energies for D1 and A1 (see table 2). Although what can be inferred from ground state calculations correlates with experimental observations, because of the non-equilibrium nature of the charge transfer process, quantum dynamic calculations are more suitable and provides a detail picture of the this mechanism. It is worth mentioning that the charge-transfer dynamics shown in this work, as a result of the explicit interaction between the monochromatic electric field and the aggregate does not include nuclear motion coupled to the electron dynamics. In particular, the decoherence effect inducing irreversible charge separation and long-lived charge-transfer state is completely absent in our model. The inclusion of nuclear dynamic in order to study the charge separation processes in light-harvesting molecular triads and in dye-sensitized solar cells has been recently formulated in^{33,34}. A lot of information can however be obtained from the relatively short time dynamics that can be studied without including nuclear motion. As mentioned in the methods section, our group has used studied the charge injection mechanism in dye-nanoparticles complexes in time domain, leading to good agreement with experimental results²⁴⁻²⁶. In this context, this work sheds new light on the photoinduced charge transfer process that underpins these novel organic nanofibril heterojunctions. Figure 4 displays the evolution of the Mulliken charge distribution in D1 and A1, upon the photoexcitation of D1+A1 complex with a sinusoidal time-dependent electric field perturbation at 533 nm and with an intensity of 0.01 V/Å. At this frequency the acceptor molecule is absorbing the energy from the field (see figure 3) and from figure 4 we can observed that the A1 molecule becomes increasingly negatively charged as a function of time. It is important to note that the net charge transfer process begins after the 40 fs, this can be interpreted as the A1 molecule requires a time interval to populate the excited state (depopulate the ground state) and thereby the D1 molecule can begin to transfer charge to this state. It is worth noting that this charge behavior throughout time occurs in a noncovalent bonded system. In order to sample the complex configuration space we have used a Born-Oppenheimer molecular dynamics scheme to sample the configuration space of A1+D1, in order to study the dependence of the aggregate geometry. The simulation was performed with the DFTB+ code¹⁷, for 25 ps with time step of 0.25 fs at 500 K. This choice of temperature provides better configuration sampling since the molecules are quite rigid. We have calculated the RMS of the trajectory giving an average value of 0.37 Å, this is the average atomic motion with respect to their equilibrium positions at the configurations obtained. Then we chose fifteen random configurations from an equilibrated trajectory and compute the electron dynamics for each sample. Finally, the charge dynamics is computed as an average of the results obtained for each of these configuration and the results are shown in Figure 5. The inner lines correspond to the mean charge of the acceptor (red) and the mean charge of the

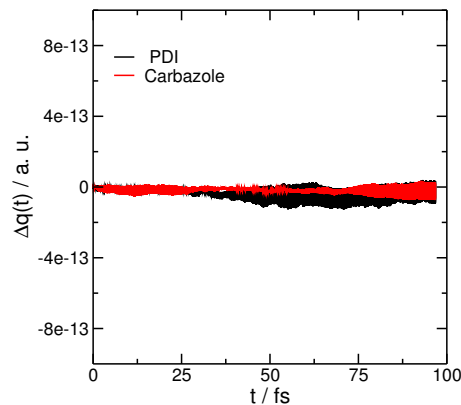


Fig. 6 Charge vs t for the system donor+acceptor without hydrocarbon chains.

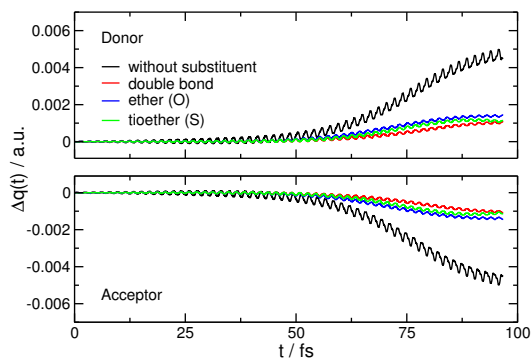


Fig. 7 Charge transferred as function of time for different aggregates with different substituents in the alkyl chain of the donor.

donor (blue). The translucent surface represents the standard deviation of the means (as $\bar{x} \pm \sigma$). The charge dynamics calculation in Figure 6 clearly shows that there is a net charge transfer from the donor to the acceptor, independently of the molecular configuration. Hence, the results shown are not due to a particular molecular configuration and are independent of the aggregates geometry to the extent explored by the performed sampling.

Another point that was discussed in Zang and co-workers¹⁵ article was that the alkyl chains not only enable effective adsorption of donor molecules on the acceptor molecules but they might play an important role in the efficiency of the charge transfer mechanism of these systems. For this reason we have studied the influence of the alkyl chain in the charge transfer process. First we have calculated the Mulliken charge change with respect to the ground state value in A1 and D1 without the hydrocarbon chains ($R = H$, see figure 1), the distance between the molecules is the same as for the A1+D1 aggregate when a sinusoidal electric field is applied to the entire complex. This situation is represented in figure 6, where no net charge transfer occurs, implying that the hydrophobic interaction between alkyl side-chains enables an effective charge transfer process between the donor and the acceptor.

Later, we study the influence of different substituents in the hydrocarbon chains. We began studying the variation of the charge transfer process in the A1+D1 complex when the C7 position of

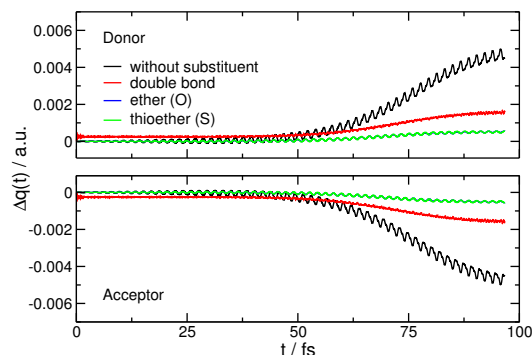


Fig. 8 Charge transferred as function of time for different aggregates with different substituents in the alkyl chain of the acceptor.

the donor chain (figure 1) is replaced by a more electronegative substituent. In figure 7 the time-evolution of the Mulliken charges are represented for different D+A complexes. This figure shows that a greater charge transfer occurs in the complex without any substituents, this is A1+D1, where the alkyl chain of the donor and the acceptor have the same chemical structure. When the C7 position is replaced by an oxygen or sulphur atom, or a double bond is inserted between positions C7 and C8 in the hydrocarbon chain, in all cases a significant decrease of the charge transfer is observed. The decrease in the value of the transferred charge of D+A complex with substituted chains can be explained by the geometry and overlap between the atomic orbitals. Each substituent, either an oxygen (or sulphur) atom or a double bond, has a distorted tetrahedral geometry respect to the C sp^3 hybridization. This distortion causes a decrease in the overlap between the atomic orbitals, resulting in a decrease of the charge transfer. Furthermore, within the complexes with substituted chain, the ether has the greater charge transfer, followed by the thioether and finally the double bond. This trend agrees with the substituents electronegativity order, the oxygen atom is the most electronegative, so it attracts more electrons from the core of the donor to the alkyl chain, consequently there is a greater proportion of charge to be transferred to the acceptor molecule.

The same study was performed in the acceptor alkyl chain. Figure 8 shows the variation of the charge transfer respect to different substitutions made in the hydrocarbon chain. As in the previous case, the presence of a substituent on the alkyl chain reduces the charge transfer significantly, but we can observe an inverse trend. The less electronegative substituent (double bond) has the greater charge transfer comparing with oxygen and sulphur atoms. This implies that a more electronegative acceptor alkyl chain would retain the charge from the donor for a longer period of time. Based on these results, we can establish that a substituent in any chain of the donor+acceptor complex works like a *resistance* reducing the charge that can be transferred from the donor to the acceptor.

We studied the photoinduced charge-transfer process for the A1+D1 complex with hydrocarbon chains between 9 and 18 carbon atoms (for both acceptor and donor). Figure 9 shows the charge of the acceptor as a function of time for all chain lengths. Figure shows that the largest chains (18 and 17 C atoms) have the

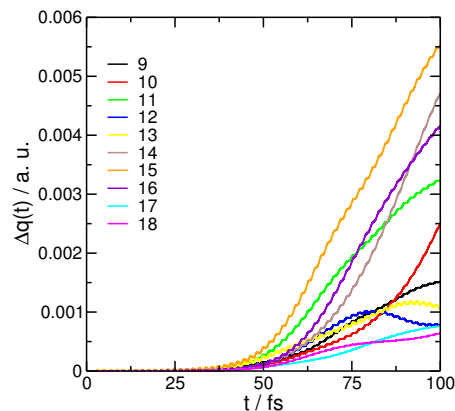


Fig. 9 Charge vs t for the system A1+D1 with different length chains (from 9 C atoms until 18 C atoms).

lowest performance, this is reasonable since the long chains represent a large tunnel barrier for the electron to surmount. Then, as the number of carbon atoms decrease the amount of charge transferred at long times increases, showing a maximum for the system with 15 C atom chains. The shorter systems are more efficient than the longest but always less than the 15 carbon atom chain. Our reasoning is that this behaviour is the result of two opposing trends. On the one hand, with shorter side chains the chromophores are closer and the coupling is larger, resulting in greater charge transfer from increased speed of formation of the electron-hole pair. On the other hand, closer distances between donor and acceptor ease electron-hole recombination, resulting in a lower charge transfer. Taking this into account, the system with 15 C atoms chains appears to be the optimal chain length for the complex. The system with 11 C atoms chains is an exception to this rule.

With the purpose to advance in the comprehension of the effective charge delocalization in these types of aggregate we extended the system including another acceptor molecule (see figure 10). Figure 10 shows the charge as function of time for each component of the system (A1 (1), A1 (2) and D1). This figure shows that the charge transfer process begins after 50 fs, the similar behavior was found in the previous system (figure 4). Also, from this plot, is possible to distinguish four steps for such process. The first step for $50 < t < 80$ fs, the charge begins to flow from the donor (D1, green line) to the first acceptor molecule (A1 (1), black line) and there is no variation of the charge in the second acceptor molecule (A1 (2), red line). Then the second step occurs for $80 < t < 100$ fs where a change in the slope of the charge function for both acceptor molecules is evidenced. The charge of A1 (1) begins to increase acquiring positive values, meanwhile A1 (2) acquires negative values indicating a net charge transfer from A1 (1) to A1 (2). For $100 < t < 118$ fs, the charge dynamics A1 (1) and A1 (2) reaches a maximum value and then both dynamics are reversed, A1 (1) begins to accept charge from A1 (2), where at $t = 118$ fs both molecule have the same charge. Finally, after $t > 118$ fs the charge of A1 (1) oscillates between negative values whereas the charge for A1 (2) oscillates between positive and negative values. Also, in figure 10 the time variation of the Mulliken charges

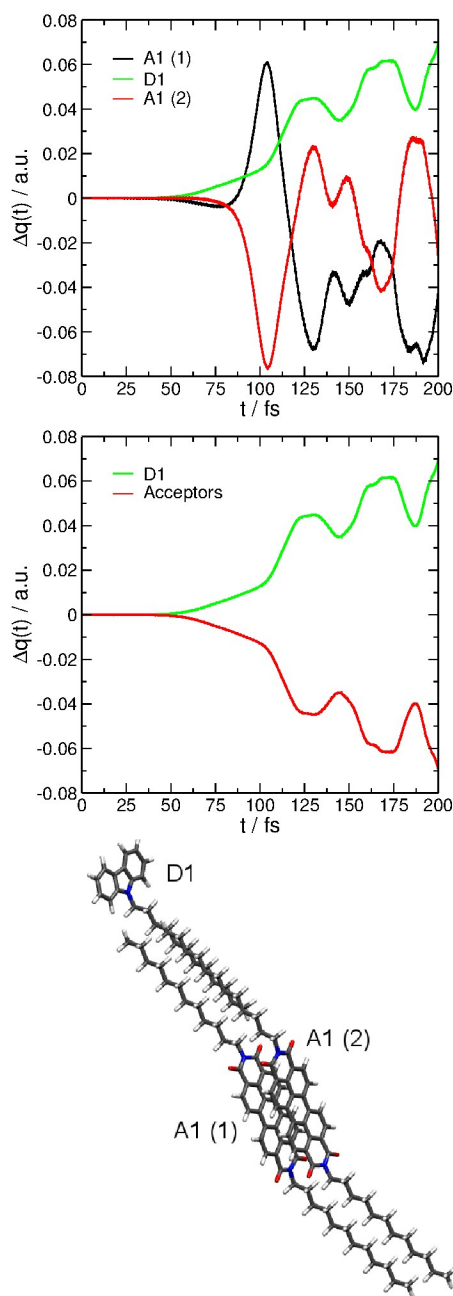


Fig. 10 (Top) Time dependent variation of the charge for A1 (1), A1 (2) and D1 interacting by London dispersion of forces. (Middle) The sum of the acceptor charges were performed to see the total charge injection to the nanofibril. (Bottom) A1(1)+A1(2)+D1 complex.

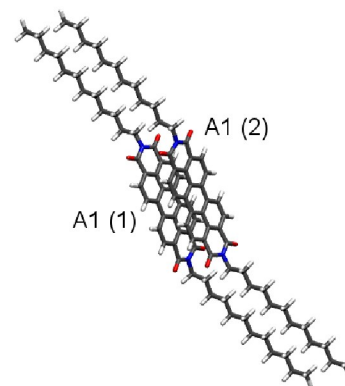
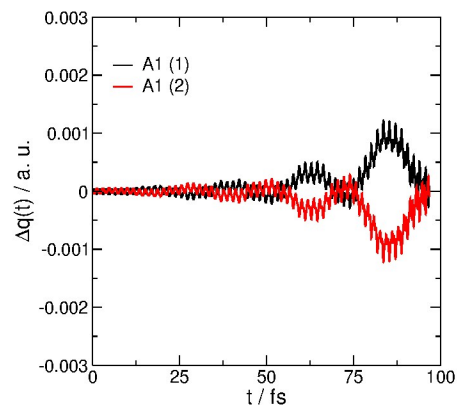


Fig. 11 (Top) Time dependent variation of the charge for two PDI derivatives. (Bottom) Two optimized PDI derivatives illustrating the $\pi - \pi$ stacking.

of the donor and the sum of the acceptors is plotted. This is other representation of the charge dynamics where it shows a clearly charge injection from the donor into the nanofiber. It is important to note that the hole is located in the donor (D1) while the electron is delocalized over both acceptor molecules.

Zang and co-workers¹⁵ reported that an aggregate of acceptor molecules interacting by π -stacking forces present negligible photocurrent under photostimulation. In order to study the importance of the presence of D1 molecules in the charge transfer mechanism, we performed the same calculation as before but without D1 molecule (figure 11). Figure 11 shows the charge of A1 (1) and A1 (2) oscillating around zero and the amplitude of the oscillation increases at longer times. This increment of the oscillation amplitudes is due to the application of the continuous laser, where the energy of the entire system is always growing. Since the energy values of the frontier molecular orbitals of each molecule are similar, there is no net driving force that favors the charge transfer mechanism to one molecule or the other, this is characterized by a cyclic variation of the charge through time. It is important to point out the observation of charge recombination in this system, in contrast, the charge recombination in the previous system is reduced for the time simulation window ($t = 200fs$) employed in this work. In addition, the magnitude of the charge values for this system is ten time lower than for the system with

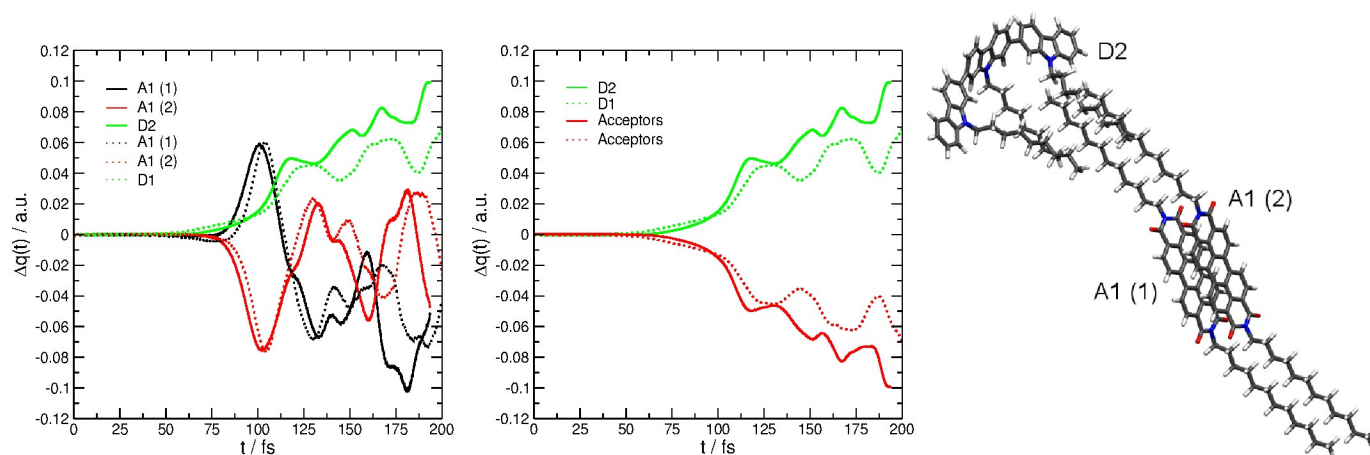


Fig. 12 (Left) Time dependent variation of the charge for two A1 molecules and D1 (dashed lines) and for two A1 molecules and D2 (solid lines). (Middle) The sum of the acceptors charge were performed to see the total charge injection to the nanofibril. (Right) Optimized A1 (1)+A1 (2)+ D2 complex.

the D1 molecule. These results implies that D1 molecule works as an electron injector to the nanofibril and promotes the charge transfer between these molecules.

For a deeper understanding in the influence of the donor molecule in the charge-transfer mechanism, we calculated the full electron dynamics of a D2 molecule (figure 1) coupled with two A1 molecules (figure 12). Figure 12 displays the time variation of the Mulliken charges for A1 (1)+A1 (2)+D2 complex, where each molecule is interacting by London dispersion of forces, and a comparison with A1 (1)+A1 (2)+D1 complex is shown. From this figure, we can observe a net charge transfer to the A1 (2) molecule in both cases although the charge value is larger for A1 (1)+A1 (2)+D2 complex. Also, we can notice that the mechanism of charge transfer for A1 (1)+A1 (2)+D2 complex is slightly different from the previous system, where a concerted charge injection from the donor molecule to the second A1 molecule is observed. This can be attributed to the three alkyl chains of D2, where this chains increases the hydrophobic interaction between the A1 molecules. From the analysis of the sum of the acceptors charge it follows that the donor D2 injects more charge to the nanofibril compared with D1 (0.1 u.a. compared to 0.07 u.a. respectively). This result is in accordance with the experimental results reported by Zang and co-workers¹⁵.

By increasing the number of acceptors molecules, we can analyze the delocalization of the charge through the entire nanofibril. With this in mind, we built a nanofiber of nearly 6 nm of length containing fifteen A1 molecules coupled with a single D2 molecule, the optimized structure is shown in figure 13. Also, in this figure is displayed the charge dynamics of the individual D2 and the sum of the charges for the A1 acceptor molecules. As in the smaller system, there is a net charge transfer from the D2 molecule to the nanofibril, but the amount of net charge transferred is higher in consequence to the system's size, where larger nanofibrils can accept more charge. Is important to note that the time evolution of the charge is slightly different for the largest system, from figure 13 we can observe a smooth behavior in the electron dynamics in comparison with the system including only two

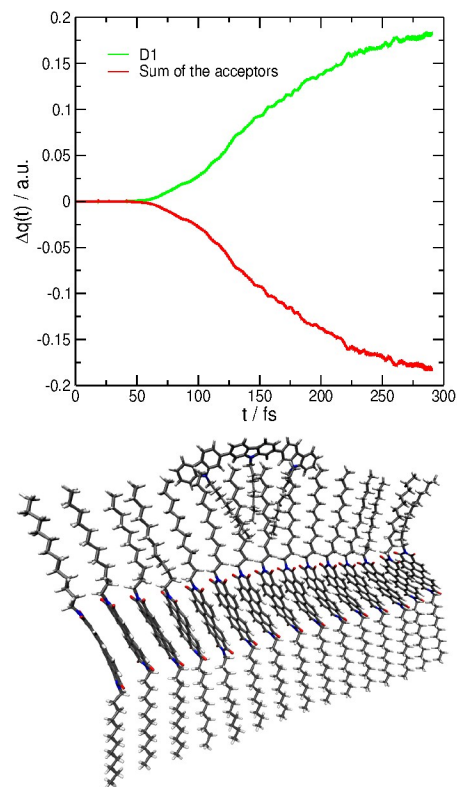


Fig. 13 (Top) Charge evolution throughout time for the system 15*A1 + D1. In order to visualize the net charge injection to the nanofibril the sum of the acceptor charges is represented. (Bottom) Optimized nanofibril of 15 A1 acceptors coupled with a D2 molecule.

acceptor molecules (figure12), which is the result of the collective electronic excitations acting in a concerted fashion between the donor and each of the acceptor molecules.

The charge transfer dynamics for each molecule is shown in figure 14 at different time values. This figure shows selected snapshots of the evolution of the $\Delta q(t)$ during the quantum dynamics simulation (the complete movie can be found in the supporting information), ranging from a positive $\Delta q(t)$ (blue) to a negative value (red), the green color implies $\Delta q(t) = 0$. At $t = 0$ fs, all molecules are colored in green meaning a neutral system. As the external electric field is turned on, at 78.0 fs we can observe that a single molecule of PDI (number 10) is absorbing the energy of the electric field, where this molecule is receiving the charge from molecule number 13. This response, is the result of the coupling between the incident electric field vector and the transition dipole moment vector of molecule number 10, where the variation of the charge in such molecule indicates a larger coupling with the laser in comparison with the other molecules. After 100 fs, it can be noticed that the negative charge is increasing in this molecule, where the PDIs of the right (number 13, 14 and 15) are transferring charge to this molecule, which is indicated by the light blue color. The observed asymmetry in the charge transfer can be explained by the electronic coupling between the molecules, where the distance between them is the smallest. During the application of the external field, the electron is located mostly in two PDIs (number 10 and 11) meanwhile the hole is delocalized over the D2 molecule and the PDIs of the ends. Finally, at $t = 283.0$ fs we can observe a transfer of the negative charge to the next PDI (number 11), where the electron is delocalized over four molecules of PDIs (number 9, 10, 11, and 12). A further observation from figure ?? is the large charge polarization in the nanofiber, the electron is localized in the center and the hole is delocalized at the edges of the nanofiber, where a clear interface is created among them, by the presence of neutral molecules (green) that enclose the electron. It is important to point out that the electron transfer across the PDIs takes place in a noncovalent system and the π -electrons are involved in the process.

4 Conclusions

In the present work we have conducted real-time quantum dynamics simulations to describe the primary charge separation process in functionalized molecular aggregates, interacting only by London dispersion forces, in order to provide detailed insights of the experimental observations reported by Zang and co-workers¹⁵.

By directly computing the time evolution of the Mulliken charge for donor-acceptor complex, we have obtained non-trivial results as the net charge transfer from donor to acceptor molecule, even when both molecules are not covalently bonded. We analyze the chemical structure of the alkyl side chain of both acceptor and donor molecules and we found that these alkyl groups work as *molecular wires* that modulate the intermolecular electron transfer, these evidences agree with the experimental findings of Zang and co-workers¹⁵.

Moreover, it is important to mention that the chemical nature of the donor molecule can enhance the amount of charge injected

to the nanofibril. Increasing the van der Waals interactions between the hydrocarbon chains, the time-dependent electron dynamics showed the generation of a stable charge-transfer complex and the recombination of the charge was reduced. By increasing the number of acceptor molecules, the quantum dynamics simulations displayed the electron transport through the nanofiber; the localization of the hole in the donor molecule as well as in the edges of the nanofiber.

The results presented in this work and in conjunction with the experimental evidence reported by Zang and co-workers¹⁵, contribute to the scientific understanding of the charge transport mechanism in noncovalent molecular aggregates. These results validate our computational method for the design of new photovoltaic material.

5 Acknowledgments

We acknowledge support by Consejo Nacional de Investigaciones Científicas y Técnicas (CONICET) through grant PIP 112-201101-0092 and wish to thank SeCyT UNC for the funding received. CRM is grateful for studentships from CONICET.

References

- 1 S. R. Puniredd, A. Kiersnowski, G. Battagliarin, W. Zajączkowski, W. W. H. Wong, N. Kirby, K. Müllen and W. Pisula, *J. Mater. Chem. C*, 2013, **1**, 2433.
- 2 P. Sonar, J. P. Fong Lim and K. L. Chan, *Energy Environ. Sci.*, 2011, **4**, 1558.
- 3 S. Lamansky, P. Djurovich, D. Murphy, F. Abdel-Razzaq, H. E. Lee, C. Adachi, P. E. Burrows, S. R. Forrest and M. E. Thompson, *J. Am. Chem. Soc.*, 2001, **123**, 4304–4312.
- 4 G. Li, R. Zhu and Y. Yang, *Nat. Photonics*, 2012, **6**, 153–161.
- 5 J. You, L. Dou, K. Yoshimura, T. Kato, K. Ohya, T. Moriarty, K. Emery, C.-C. Chen, J. Gao, G. Li and Y. Yang, *Nature communications*, 2013, **4**, 1446.
- 6 J. You, C.-C. Chen, Z. Hong, K. Yoshimura, K. Ohya, R. Xu, S. Ye, J. Gao, G. Li and Y. Yang, *Advanced Materials*, 2013, **25**, 3973–3978.
- 7 S. Günes, H. Neugebauer and N. S. Sariciftci, *Chem. Rev.*, 2007, **107**, 1324–1338.
- 8 S. M. Falke, C. A. Rozzi, D. Brida, M. Maiuri, M. Amato, E. Sommer, A. De Sio, A. Rubio, G. Cerullo, E. Molinari and C. Lienau, *Science*, 2014, **344**, 1001–5.
- 9 Y. He and Y. Li, *Phys. Chem. Chem. Phys.*, 2011, **13**, 1970–1983.
- 10 Y. Lin and X. Zhan, *Mater. Horizons*, 2014, **1**, 470.
- 11 X. Zhang, Z. Lu, L. Ye, C. Zhan, J. Hou, S. Zhang, B. Jiang, Y. Zhao, J. Huang, S. Zhang, Y. Liu, Q. Shi, Y. Liu and J. Yao, *Adv. Mater.*, 2013, **25**, 5791–7.
- 12 L. Zang, Y. Che and J. Moore, *Acc. Chem. Res.*, 2008, **41**, 1596–1608.
- 13 F. S. Kim, G. Ren and S. a. Jenekhe, *Chem. Mater.*, 2011, **23**, 682–732.
- 14 J. Hyoung Park, A. R. Carter, L. M. Mier, C.-Y. Kao, S. a. M. Lewis, R. P. Nandiyala, Y. Min and A. J. Epstein, *Appl. Phys. Lett.*, 2012, **100**, 073301.

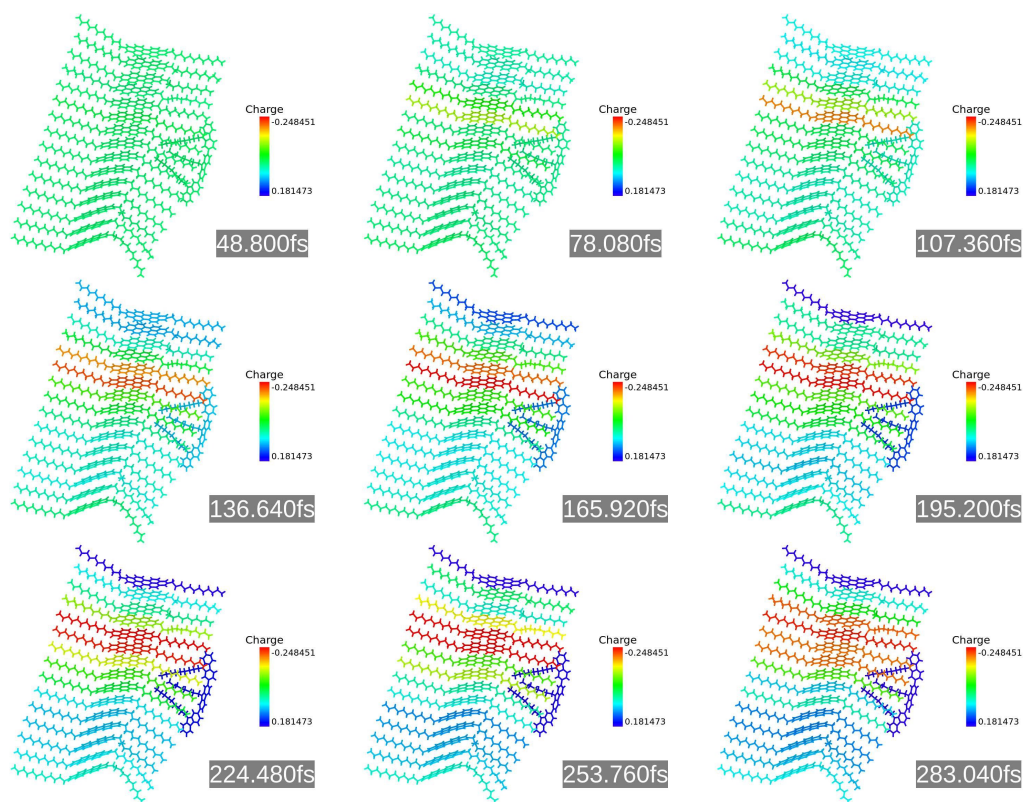
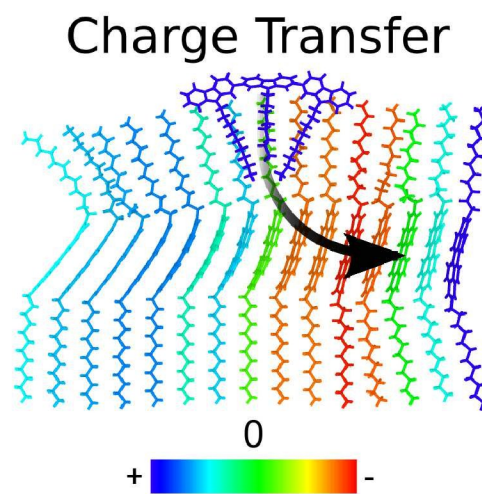


Fig. 14 Intensity plot of the net charge per molecule at 9 different times, in correspondence with the charge dynamics show in 13

- 15 Y. Che, H. Huang, M. Xu, C. Zhang, B. R. Bunes, X. Yang and L. Zang, *J. Am. Chem. Soc.*, 2011, **133**, 1087–91.
- 16 M. Elstner, D. Porezag, G. Jungnickel, J. Elsner, M. Haugk, T. Frauenheim, S. Suhai and G. Seifert, *Physical Review B*, 1998, **58**, 7260–7268.
- 17 B. Aradi, B. Hourahine and T. Frauenheim, *The journal of physical chemistry. A*, 2007, **111**, 5678–84.
- 18 T. Niehaus, M. Elstner, T. Frauenheim and S. Suhai, *J. Mol. Stru.: {THEOCHEM}*, 2001, **541**, 185 – 194.
- 19 M. Gaus, Q. Cui and M. Elstner, *J. Chem. Theory Comput.*, 2011, **7**, 931–948.
- 20 M. B. Oviedo, C. F. a. Negre and C. G. Sánchez, *Physical chemistry chemical physics : PCCP*, 2010, **12**, 6706–11.
- 21 M. B. Oviedo and C. G. Sánchez, *J. Phys. Chem. A*, 2011, **115**, 12280–12285.
- 22 E. N. Primo, M. B. Oviedo, C. G. Sánchez, M. D. Rubianes and G. A. Rivas, *Bioelectrochemistry*, 2014, **99C**, 8–16.
- 23 V. C. Fuertes, C. F. a. Negre, M. B. Oviedo, F. P. Bonafé, F. Y. Oliva and C. G. Sánchez, *Journal of physics. Condensed matter : an Institute of Physics journal*, 2013, **25**, 115304.
- 24 C. F. a. Negre, V. C. Fuertes, M. B. Oviedo, F. Y. Oliva and C. G. Sánchez, *The Journal of Physical Chemistry C*, 2012, **116**, 14748–14753.
- 25 M. B. Oviedo, X. Zarate, C. F. A. Negre, E. Schott, R. Arratia-Pérez and C. G. Sánchez, *The Journal of Physical Chemistry Letters*, 2012, **3**, 2548–2555.
- 26 C. F. A. Negre, K. J. Young, M. B. Oviedo, L. J. Allen, C. G. Sánchez, K. N. J. J. B. Benedict, R. H. Crabtree, P. Coppens, G. W. Brudvig and V. S. Batista, *J. Am. Chem. Soc.*, 2014, **136**, 16420–16429.
- 27 A. Stukowski, *Modelling and Simulation in Materials Science and Engineering*, 2010, **18**, 015012.
- 28 W. Humphrey, A. Dalke and K. Schulten, *Journal of Molecular Graphics*, 1996, **14**, 33–38.
- 29 J. Stone, *M.Sc. thesis*, Computer Science Department, University of Missouri-Rolla, 1998.
- 30 H. Walba and G. E. K. Branch, *Journal of the American Chemical Society*, 1951, **73**, 3341–3348.
- 31 W. E. Ford and P. V. Kamat, *The Journal of Physical Chemistry*, 1987, **91**, 6373–6380.
- 32 M. Elstner, P. Hobza, T. Frauenheim, S. Suhai and E. Kaxiras, *J. Chem. Phys.*, 2001, **114**, 5149–5155.
- 33 L. G. C. Rego, B. C. Hames, K. T. Mazon and J. O. Joswig, *Journal of Physical Chemistry C*, 2014, **118**, 126–134.
- 34 A. Monti, C. F. a. Negre, V. S. Batista, L. G. C. Rego, H. J. M. de Groot and F. Buda, *The Journal of Physical Chemistry Letters*, 2015, 2393–2398.

6 Graphical Abstract



Real-time atomistic simulation of photoexcited exciton dynamics in non-covalently bonded perylene diimides aggregates.